the FEBS Journal
EDITOR'S CHOICE

The intramolecular disulfide-stapled structure of laterosporulin, a class IId bacteriocin, conceals a human defensin-like structural module

Pradip Kumar Singh[1], Vipul Solanki[2], Shalley Sharma[1], Krishan Gopal Thakur[2], Beena Krishnan[2] and Suresh Korpole[1]

1 Microbial Type Culture Collection & Gene Bank, CSIR-Institute of Microbial Technology, Chandigarh, India
2 G.N. Ramachandran Protein Centre, CSIR-Institute of Microbial Technology, Chandigarh, India

Keywords
bacteriocin; defensin; microscopy; nonmultiplying cells; X-ray crystallography

Correspondence
K. G. Thakur, B. Krishnan & S. Korpole, Council of Scientific and Industrial Research-Institute of Microbial Technology, Chandigarh-160036, India.
Fax: +91-172-2690632/2695215
Tel.: +91-172-6665470; +91-172-6665468; +91-172-6665159
E-mails: krishang@imtech.res.in; beena@imtech.res.in; suresh@imtech.res.in

(Received 12 August 2014, revised 16 October 2014, accepted 21 October 2014)

doi:10.1111/febs.13129

The growing emergence of antibiotic-resistant bacteria has led to the exploration of naturally occurring defense peptides as antimicrobials. In this study, we found that laterosporulin (LS), a class IId bacteriocin, effectively kills active and nonmultiplying cells of both Gram-positive and Gram-negative bacteria. Fluorescence and electron microscopy suggest that growth inhibition occurs because of increased membrane permeability. The crystal structure of LS at 2.0 Å resolution reveals an all-β conformation of this peptide, with four β-strands forming a twisted β-sheet. All six intrinsic cysteines are intramolecularly disulfide-bonded, with two disulfides constraining the N terminus of the peptide and the third disulfide crosslinking the extreme C terminus, resulting in the formation of a closed structure. The significance of disulfides in maintaining the in-solution peptide structure was confirmed by CD and fluorescence analyses. Despite a low overall sequence similarity, LS has disulfide connectivity [C^{I}–C^{V}, C^{II}–C^{IV}, and C^{III}–C^{VI}] like that of β-defensins and a striking architectural similarity with α-defensins. Therefore LS presents a missing link between bacteriocins and mammalian defensins, and is also a potential antimicrobial lead, in particular against nonmultiplying bacteria.

Database
The atomic coordinates and the structure factors have been deposited in the Protein Data Bank under accession number 4OZK

Introduction

An effective treatment of any infection necessitates killing all forms of the causative pathogen, because quiescent states of viable bacteria, i.e. dormancy and/or a nonmultiplying state, is one of the major causes of chronic infection and prolonged antibiotic treatment [1,2]. Most antibiotics target metabolic processes in bacteria, and are ineffective against such quiescent cells. As cell membranes constitute the first line of defense against external killing agents, antimicrobials that target membrane(s) are promising candidates for killing bacteria in all of their forms. Remarkably, the majority of naturally occurring defense peptides are

Abbreviations
Amp, ampicillin; AMP, antimicrobial peptide; CFU, colony-forming unit; CTC, 5-cyano-2,3-ditolyl tetrazolium chloride; DAPI, 4,6-diamidino-2-phenylindole; HBD, human β-defensin; HD, human defensin; HNP, human neutrophil peptide; MIC, minimum inhibitory concentration; NS, nisin; P_2, poly-proline II; PDB, Protein Data Bank; PMB, polymyxin B; RBC, red blood cell; TEM, transmission electron microscopy; TCEP, Tris(2-carboxyethyl)phosphine.

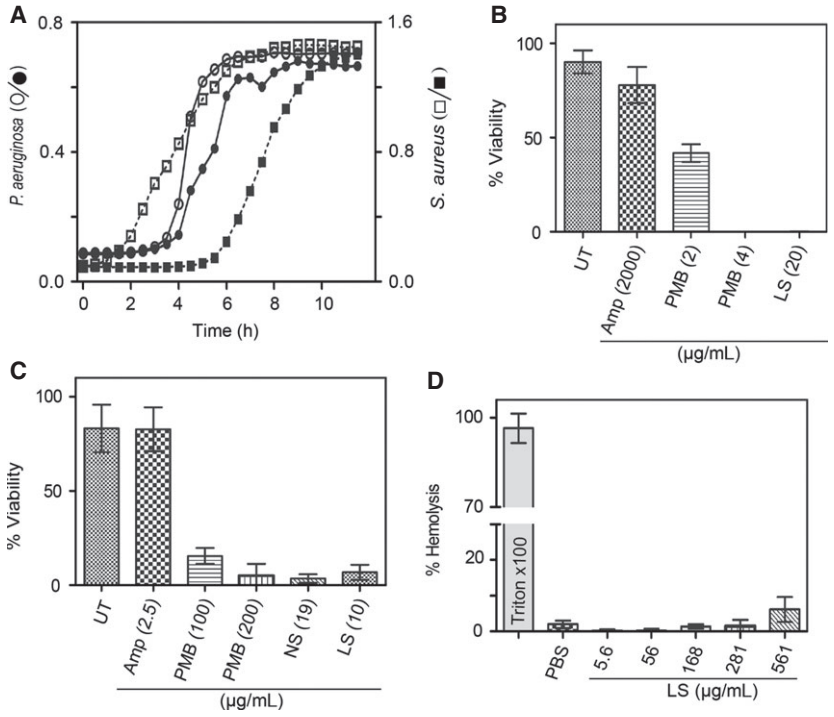

Fig. 1. LS kills nonmultiplying bacteria and has no adverse effect on mammalian RBCs. (A) Comparative growth curves of active (open symbols) and nonmultiplying (filled symbols) cells of *P. aeruginosa* (circles) and *S. aureus* (squares). (B, C) Cell viability was used as a measure of the effect of LS on nonmultiplying cells of *P. aeruginosa* (B) and *S. aureus* (C). The numbers in parentheses in (B) and (C) denote the concentration ($\mu g \cdot mL^{-1}$) used in the experiment. The CFU count from the untreated sample (UT) was taken as 100% in the cell viability calculations. (D) LS toxicity to mammalian cells was assayed by measuring hemolytic activity of the peptide. Amp, PMB, NS, Triton X-100 and PBS served as controls. Representative data with error bars obtained from triplicate measurements are shown.

known to target bacterial membrane, and consequently offer a repertoire of potential antimicrobials against all the different stages of bacteria. The likelihood of bacteria developing resistance to such antimicrobial peptides (AMPs) is generally deemed to be low [3]. Therefore, AMPs are being considered as alternatives for targeting multidrug-resistant and opportunistic pathogens [4–6], and several AMPs are already in different phases of drug development [5,6].

AMPs are produced by all organisms as a part of their innate defense system. These antibiotic-like peptides show extreme diversity in their sequence composition, structure, target specificity, and mode of action [7,8]. Whereas cysteine-rich cationic defensins, i.e. α, β, and θ, are important components of the host immune response against infection in eukaryotes [9], bacteriocins, i.e. class I (lantibiotics) and class II (unmodified, a–e), actively participate in removing microbial competition in prokaryotes [10]. Effective exploitation of AMPs as drug molecules will be vastly aided by comprehensive knowledge of structure–function relationships of AMPs.

Here, we report on laterosporulin (LS), a cysteine-rich heat-stable 49-residue peptide secreted by *Brevibacillus* sp. strain GI-9 [11], which shows broad-spectrum killing of vegetative and nonmultiplying cells of both Gram-positive and Gram-negative bacteria. Microscopic imaging of peptide-treated cells points to the cell membrane as a target of LS. We have solved the crystal structure of LS at high resolution (2 Å), which revealed that the peptide assumes a four-strand twisted β-sheet structure stabilized by three intramolecular disulfide bridges. The disulfides and extensive interaction network present in the monomer underlie the extreme stability observed for such a short peptide. Crystal packing analysis also suggests the probability of the molecule trimerizing by intermolecular β-sheet expansion. Structural analysis allowed us to unmask the structural homology between LS and human defensins (HDs). The structure of LS thus highlights the evolutionary conservation of the defensin-like sequence and fold in bacteria.

Results

LS is effective against nonmultiplying bacteria

In a previous study, LS was reported to be a broad-spectrum antibacterial peptide [11]. Here, we tested its activity against nonmultiplying cells. The bacterial strains *Pseudomonas aeruginosa* MTCC 1934 and *Staphylococcus aureus* MTCC 1430 were used as reference strains to generate long-term nonmultiplying cells of Gram-negative and Gram-positive bacteria, respectively. An increased lag phase as compared with vegetative cells of the same organism in a regrowth experiment (Fig. 1A) and tolerance to antibiotics such as ampicillin (Amp) (Fig. 1B,C), rifampicin, and tetra-

cycline (data not shown), along with sensitivity to polymyxin B (PMB) and nisin (NS) (Fig. 1B,C), confirmed the nonmultiplying state of the culture. As expected, the revived culture of these cells resumed sensitivity to antibiotics at the expected minimum inhibitory concentration (MIC) values determined for corresponding vegetative cells, suggesting that no additional antibiotic resistance was acquired through any genetic modification during dormancy.

Similarly to PMB, LS was found to kill nonmultiplying cells of both *P. aeruginosa* and *S. aureus* (Fig. 1B,C). LS was found to be equally effective in killing both vegetative and nonmultiplying cells of *P. aeruginosa*, with comparable extents of killing being observed at similar MICs. However, nonmultiplying cells of *S. aureus* showed more tolerance to LS, with 10% cell viability being observed at 10 × MIC (data not shown). Nonetheless, comparison of absolute concentrations indicated that LS killed vegetative and nonmultiplying cells of *S. aureus* at two-fold lower concentrations than were needed to kill *P. aeruginosa*. More notably, LS, with effective killing of > 90% of nonmultiplying *S. aureus* cells at 10 $\mu g \cdot mL^{-1}$, was as effective as NS and at least 10-fold more potent than PMB, the known dormant cell inhibitors.

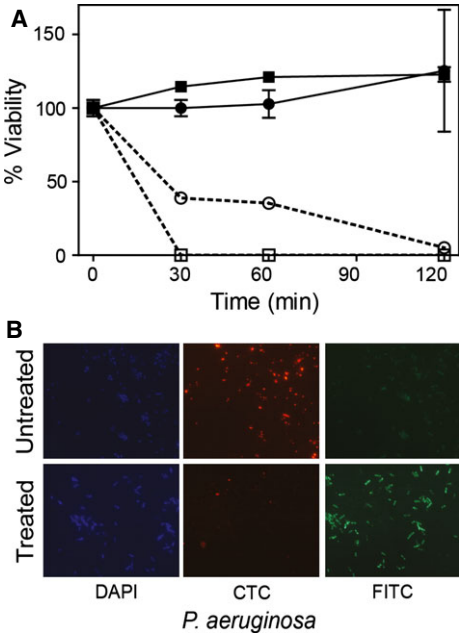

Fig. 2. LS targets cell membrane. (A) LS-mediated killing kinetics of *P. aeruginosa* (circles) and *S. aureus* (squares) cells. Untreated (filled symbols) active cultures (0.25 mL) were treated with 5 X MIC (open symbols) of LS, and CFUs were counted at 30, 60 and 120 min to determine the time dependence of bactericidal activity. MIC values were estimated with the microtiter plate method, as described previously [11]. (B) Fluorescence microscopic images of untreated and peptide-treated cells of *P. aeruginosa* stained with CTC and FITC, showing metabolically active and membrane-compromised cells, respectively. The blue fluorescence from DAPI staining indicates cells present in the field of view. Green fluorescence indicates inner membrane permeation by FITC, and an absence of red fluorescence suggests that LS-treated cells are metabolically inactive.

In order to check whether LS is toxic to mammalian cells, we assayed its hemolytic activity, if any. It was observed that LS had practically no effect on red blood cells (RBCs) at concentrations at which it kills vegetative and nonmultiplying cells of *P. aeruginosa* and *S. aureus*, and < 10% hemolysis was observed only at very high concentrations of ~ 0.5 $mg \cdot ml^{-1}$ (Fig. 1D).

Cell membrane permeability is altered by LS

Fluorescence microscopy and transmission electron microscopy (TEM) were performed on LS-treated cells to obtain insights into its mode of action. The bactericidal kinetics of LS were determined for estimation of the concentration and incubation time for the microscopy study. The rate of cell killing with the peptide at 5 × MIC (Fig. 2A) indicated that maximum cell death was achieved with 2 h of treatment. Enhanced activity of LS against *S. aureus* relative to *P. aeruginosa* was further manifested by a rapid increase in killing rate, with nearly 100% cell death within 30 min at 5 × MIC for *S. aureus*.

FITC is a small (389 Da) green fluorescent dye known to be impermeable to intact cell membranes, and absorption of FITC into the cell is thus indicative of any damage/modification/sensitization of the cell membrane. Uniform green fluorescence was observed in both *P. aeruginosa* (Fig. 2B) and *S. aureus* (data not shown) cells only after treatment with LS. Additionally, the absence of red fluorescence after 5-cyano-2,3-ditolyl tetrazolium chloride (CTC) (a dye that indicates the metabolic status of cells) staining of LS-treated *P. aeruginosa* cells indicated that the treated cells were metabolically inactive. Finally, blue fluorescence from cells stained with 4,6-diamidino-2-phenylindole (DAPI) (DNA-binding dye) [12] provided evidence that there was no DNA leakage from LS-treated cells (Fig. 2B). The treated cells thus seem to maintain cell shape at early time points of treatment, and complete cell lysis ensues at later treatment time points, as is also evident from the electron microscopy images [11].

To capture the effect of early interactions of LS with cells, we obtained transmission electron micrographs of both *P. aeruginosa* and *S. aureus* cells treated with sublethal concentrations for shorter time periods (60 min). A change in membrane morphology,

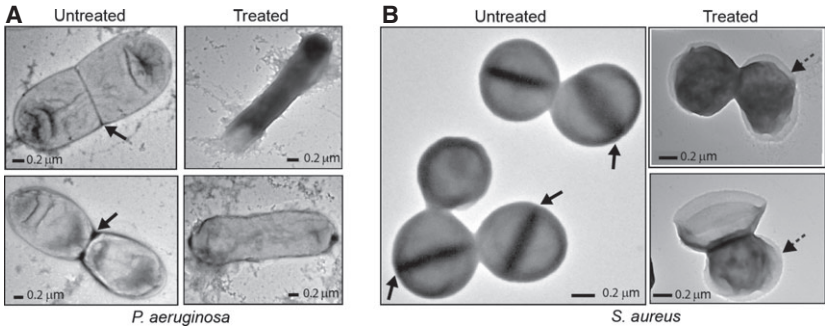

Fig. 3. Effect of LS treatment on *P. aeruginosa* (A) and *S. aureus* (B) cells monitored by negative staining TEM. The solid arrow represents the cell division plate, and the broken arrow in (B) represents the halo observed in many of the LS-treated cells. Increased darkness in the treated cells indicates entry of the phosphotungstic acid stain, and is a reflection of compromised cell membrane.

with increased roughness, was observed in peptide-treated cells (Fig. 3). The presence of LS inhibited cell division, as marked by an absence of the cell division plate in both cell types (marked by black arrows in Fig. 3). Additionally, a distinct halo was observed around most of the peptide-treated *S. aureus* cells, which we speculate may be the degraded cell wall (marked by dashed arrows in Fig. 3B). Treated cells of both *P. aeruginosa* and *S. aureus* appeared dark, owing to the cytoplasmic entry of phosphotungstic acid stain, again suggesting inner membrane permeabilization.

The LS monomer adopts an all-β structure with disulfide-constrained termini

The peptide crystallized in space group $P4_332$, having only one molecule in the asymmetric unit and 39% solvent content. Despite their small size (< 40 μm), crystals diffracted to ~ 2.0 Å resolution at home source (Table 1). The analyses of native and iodine derivative crystals showed that there were no significant differences in the peptide structure at pH 8.3 and pH 4.6. All 49 residues of the secreted peptide were resolved in the electron density map. LS adopts an all-β structure, with four β-strands, i.e. β1 (8–15), β2 (18–20), β3 (24–35), and β4 (38–50), forming a twisted β-sheet resulting in an elongated rod-like structure with dimensions of ~ 40 × 14 Å (Fig. 4A). The crystal structure reveals that all six intrinsic cysteines are present in an oxidized state, with intramolecular disulfide bond connectivity of Cys3–Cys42, Cys5–Cys34, and Cys19–Cys50 (C^{I}–C^{V}, C^{II}–C^{IV}, and C^{III}–C^{VI}) (Fig. 4A, B). Although the first four residues of the N terminus (Ala2 to Cys5) are in an extended conformation, this segment remains constrained by two disulfide bonds (Cys3–Cys42 and Cys5–Cys34) and backbone hydrogen bonding between Ala2-NH_2 and Cys42-CO of strand β4 (Fig. 4C,D). The peptide C terminus is also constrained by the Cys19–Cys50 disulfide. The structure is stabilized by several hydrophobic interactions,

Table 1. Data collection and refinement statistics.

	Native	Iodine derivative
PDB code	4OZK	
Data collection		
Space group	$P4_332$	$P4_332$
Cell dimensions		
a, *b*, *c* (Å)	65.00, 65.00, 65.00	64.69, 64.69, 64.69
α, β, γ (°)	90, 90, 90	90, 90, 90
Resolution (Å)	45.96–2.04 (2.14–2.04)[a]	45.74–2.04 (2.14–2.04)
R_{merge}	0.110 (0.436)	0.096 (0.349)
$I/\sigma I$	17.0 (5.3)	15.7 (6.1)
Completeness (%)	98.9 (92.8)	98.1 (88.2)
Redundancy	10.5 (10.3)	5.4 (4.8)
Radiation source	Home source, Cu Kα	
Wavelength (Å)	1.5418	
Refinement		
Resolution (Å)	29.07–2.04	
No. of reflections	3302	
R_{work}/R_{free}	0.1962/0.2274	
No. of atoms		
Protein	388	
Water	23	
B-factors		
Protein	24.19	
Water	22.50	
Rmsd		
Bond lengths (Å)	0.007	
Bond angles (°)	1.049	
Structure validation		
Ramachandran plot statistics		
Most favored (%)	97.87	
Allowed regions (%)	2.13	
Disallowed region (%)	0	

[a] Values in parentheses are for the highest-resolution shell.

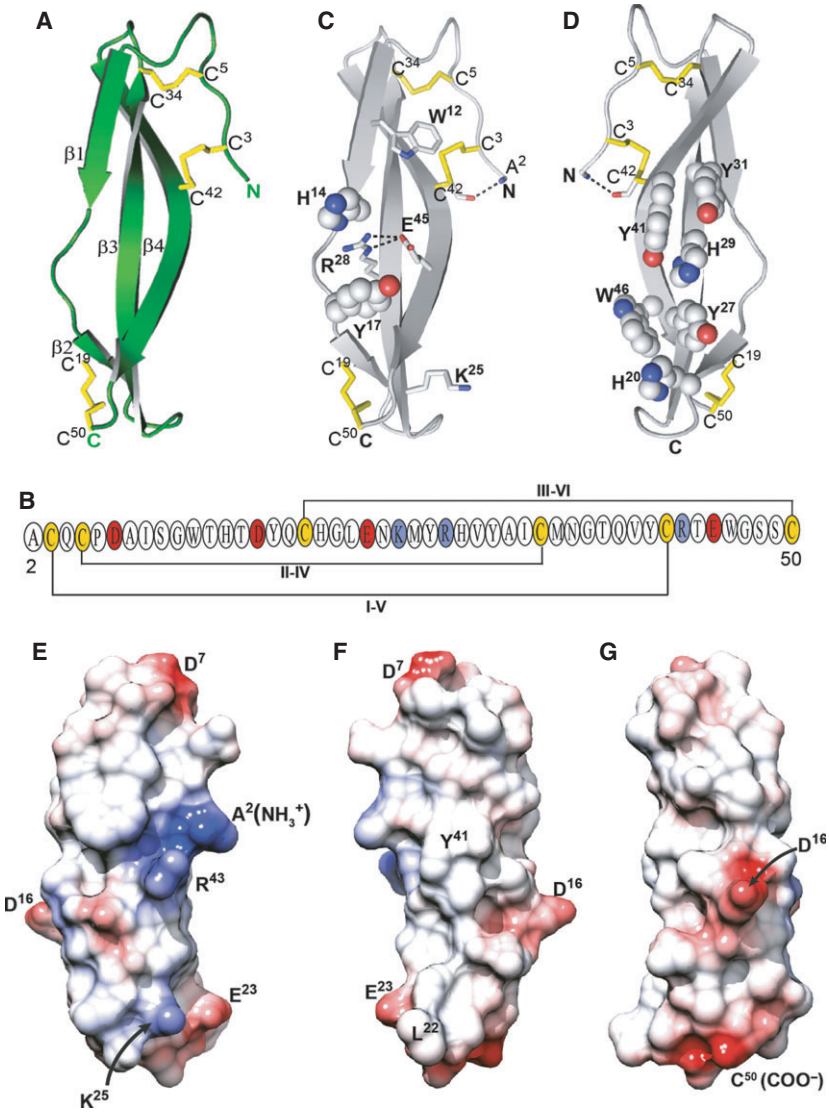

Fig. 4. LS assumes an all-β structure. (A) Cartoon representation of the LS monomer (PDB: 4OZK), showing secondary structural elements. (B–D) The amino acid sequence and defensin-like disulfide connectivity in the LS sequence are shown in (B). The cysteine, acidic and basic residues in the sequence are colored in yellow, red, and blue respectively. Intramolecular disulfide bonds (yellow sticks) and the extensive interaction network stabilizing the structure are shown in (C) and (D). The N terminus and C terminus are marked as N and C, respectively. (E–G) Electrostatic surface potential of the monomer reveals localized distribution of charges on the peptide surface. The surface representation shown is electrostatic surface coloring produced by UCSF CHIMERA [41] with the 'Coulombic surface coloring' function and default parameters ($\varepsilon = 4r$ and threshold of $\pm$ 10 kcal·mol^{-1}).

main chain–side chain hydrogen bonds, and side chain–side chain hydrogen bonds [13]. Additional notable polar interactions include an Arg28–Glu45 salt bridge, cation–π interactions of Arg28–His14 and Arg28–Tyr17, two distinct aromatic stacking clusters of His29–Tyr31–Tyr41 and His20–Tyr27–Trp46, and a sulfur–aromatic interaction between Cys42 and Trp12 (Fig. 4C,D). Such an extensive interaction network and the disulfide bridging in the structure suggests high thermodynamic stability of the peptide. Electrostatic surface analysis of LS revealed an amphipathic nature of the β-structure. Whereas Ala2(NH_3^+), Arg43 and Lys25 contribute to two positively charged protrusions on one face of the peptide (Fig. 4E), the other face is relatively apolar, with a slightly concave surface (Fig. 4F). Furthermore, there are three distinct localized negative patches contributed by Asp7 and Asp16, located on the top and middle, respectively, and Glu23 and Cys50(COO^-) at the bottom end of the molecule (Fig. 4G).

Crystal contact analysis reveals possible trimerization in LS mediated by intermolecular β-sheet expansion

Crystal-packing analysis suggests a possible tripod-like trimeric state of the peptide (Fig. 5A). A total of ~ 1000 Å^2 of solvent-accessible surface area is buried upon trimerization. In total, the overall trimeric association is stabilized by 15 interchain hydrogen bonds, three salt bridges, a Trp12 aromatic cluster, and several other nonbonded interactions (Fig. 5B). The most

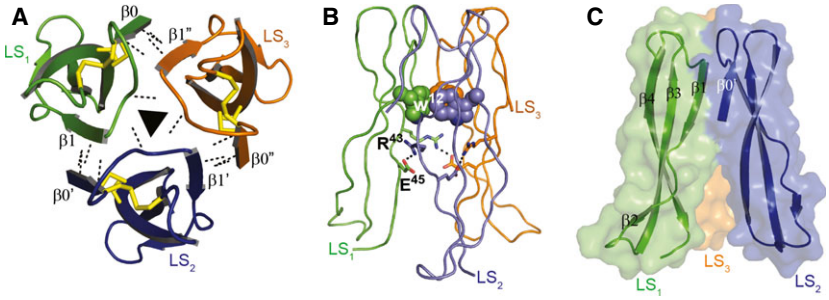

Fig. 5. Trimeric assembly of LS in the crystal structure. (A) Crystal contact analysis shows that oligomerization of LS mediated by intermolecular association of strands β1 and β0′ is stabilized by alternating intramolecular disulfide bridges (yellow sticks) and intersubunit hydrogen bonds (black dotted lines). The β-strand labeled as 'β0′ is formed from the N-terminal residues Ala2 to Cys5, which engage in the intermolecular backbone-mediated hydrogen-bonding with strand β1 only in the context of a crystallographic trimer, and the prime and double prime symbols refer to the strand contribution from/to a different monomer in the trimeric assembly. (B) Stabilizing Trp cage-like interactions formed by Trp12 (spheres), and the intersubunit salt bridge (dotted lines) between Glu45 and Arg43 (sticks) at the core of trimeric LS are shown. (C) The intermolecular β-sheet expansion observed in the trimer. The surface representation also highlights the tripod-like architecture of the LS trimer. The monomeric units are represented as $LS_{1–3}$.

noticeable and significant conformational transition is seen in the first four N-terminal residues of the peptide. Ala2 to Cys5, occurring as a structurally constrained coil in the monomer, transition to form a β-strand, β0′ (the prime symbol here refers to contribution from/to a different molecule), and participates in backbone hydrogen bonding with strand β1 of its neighboring subunit in the trimer. The topology of the expanded β-sheet thus formed in a trimer is β0′β1β2β3β4 (Fig. 5C). Trimerization is accompanied by the formation of a tightly packed hydrophobic core burying Ala8, Ile9, Trp12, Val30, Val40 and Cys5–Cys34 from each monomer. A 'Trp-cage'-like motif formed by Trp12 from each monomer in the central core and intermolecular salt bridge interactions between Arg43 and Glu45 emerge as key stabilizing interactions in the trimer (Fig. 5B).

The trimeric organization in LS resembles a tripod, with the intermolecular spacing similar to a tripod leg-spacing leading to wide sideways gaps and a fully solvent-accessible large opening at the bottom of the structure (Fig. 5C). Such an assembly creates a unique charge distribution in the LS trimer. The central cavity formed is polar, with a net positive charge contributed by Ala2(NH_3^+), Lys25, Arg28, and Arg43, and it conjoins the top portion of the structure at the Trp12 aromatic cage. In contrast, the outer surface of the trimer shows negatively charged patches from Asp7, Asp16, Glu23, and Cys50 (COO^-).

The in-solution conformation of LS is in concordance with its crystal structure

A series of biochemical and biophysical experiments were carried out to assess the LS conformation in solution. The involvement of all six cysteines in intramolecular disulfide linkages was confirmed by MALDI-TOF MS of the native and tris(2-carboxyethyl)phosphine (TCEP)-reduced peptide. A simple observation of visible precipitation upon reduction of disulfides at higher peptide concentrations gave the earliest clue regarding the importance of disulfides to the structure.

The key role of disulfides in maintaining the LS structure in solution was conclusively supported by far UV–CD (Fig. 6A) and intrinsic fluorescence (Fig. 6B) analyses of the reduced peptide. An atypical CD spectrum was observed for the native peptide,

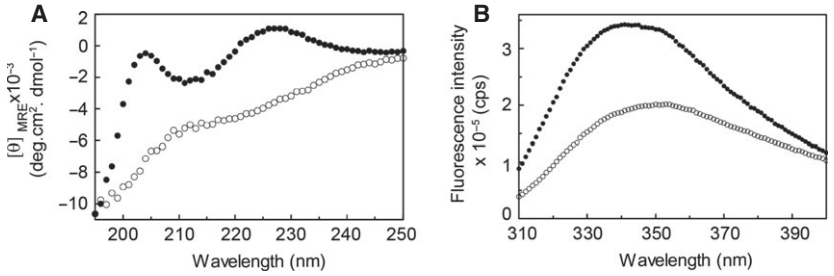

Fig. 6. Disulfides are critical to the native structure (filled circle) of LS in solution. Reduction of disulfides (open circle) causes significant structural changes in both the secondary [(A) far-UV–CD)] and tertiary [(B) tryptophan fluorescence] structure of the peptide.

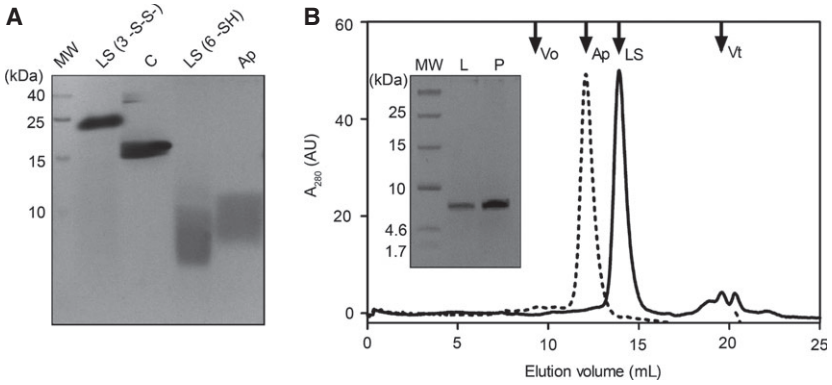

Fig. 7. Biochemical analyses of LS in solution. (A) Differential mobility of oxidized LS (3 –S-S–) and reduced LS (6 –SH) was observed by analysis of samples with 18% Tris/glycine SDS/PAGE. CRABP1 (C, 18 kDa), and aprotinin (Ap, 6.5 kDa) served as molecular mass controls. Small proteins (Ap and LS) were observed to migrate as diffuse bands on the Tris/glycine gels. (B) Size exclusion chromatography profile for LS on a Superdex peptide HR 10/300 column. The reduced samples of purified LS loaded (L) and the peak corresponding to LS eluted from the column (P) in 16% Tris/tricine SDS/PAGE [inset in (B)] show the purity of the preparation. The TCEP-reduced peptide was observed to migrate as expected according to its monomeric size in SDS/PAGE. V_o and V_t in (B) represent the void volume and the total volume of the column, respectively.

with a positive band at 228 nm, a negative band at ~ 210 nm, and an intense negative peak at ~ 195 nm. We attribute the positive band at 228 nm to extensive disulfide bonds [14] and/or the presence of aromatic interactions present in LS [15]; the negative band at ~ 210 nm is the signature band of a β-structure [16]. The presence of a deep minimum at ~ 195 nm is considered to indicate either the presence of considerable poly-proline II (P_2) content or randomness in the structure. The fine band pattern in the spectrum suggests that the negative band at 195 nm is likely to arise from a P_2 conformation in the peptide. In fact, the crystal structure shows that a significant number of residues in LS adopt the P_2 conformational space of the Ramachandran plot. LS, with an f_{P2}/f_β of 0.37, is an example of the β_{II} class of proteins that show P_2-like CD spectra despite the presence of significant β-structure content (61% in the monomer) [17]. Thus, the secondary structure obtained from analyzing multiple bands of the far UV–CD spectrum of the native peptide is in excellent agreement with the crystal structure. In contrast to the above-described well-structured spectrum observed for the native protein, the reduced peptide spectrum loses the band pattern (Fig. 6A). The disappearance of the 228 nm positive band confirms the absence of disulfide and a probable loss of aromatic packing in the structure. The contribution of the disulfide to protein stability was also indicated by the high thermal stability shown by the molecule in a CD unfolding study, wherein a 50% loss in secondary structure was observed at ~ 80 °C, and the peptide retained ~ 40% structure even at 90 °C (data not shown).

The effect of reducing disulfides in the tertiary structure of the peptide was apparent from the observed red shift in emission wavelength maximum ($\lambda_{em,max}$) from 340 nm to 350 nm and from the approximately 50% reduction in fluorescence intensity of the reduced peptide. Increased solvent exposure of the two intrinsic tryptophans (Trp12 and Trp46) and water-mediated quenching can explain the observed fluorescence of the reduced peptide. The $\lambda_{em,max}$ of 340 nm of the native peptide indicates a relatively polar environment around the tryptophan(s).

Although native (oxidized) LS showed significantly reduced electrophoretic mobility (Fig. 7A), the peptide eluted from a Superdex peptide HR 10/300 column corresponded to a size of ~ 2 kDa (Fig. 7B). Thus, size exclusion chromatography analysis of the native peptide remained inconclusive. The location of the reactive amino acids that are typically employed for crosslinking in the trimeric assembly observed in the crystal structure indicated that the bifunctional crosslinkers could not be used to trap oligomers (if any). We therefore attempted photoinduced crosslinking of unmodified proteins with tris(bipyridyl)Ru(II) complex [18] and 0.5 $mg{\cdot}mL^{-1}$ peptide, but no higher-order oligomers were observed. It can be thus inferred that LS is likely to exist predominantly as a monomer at micromolar concentrations, and trimers may occur at high concentrations, such as that achieved in crystals.

Discussion

Leaderless secretion of unmodified LS clusters it with an underrepresented but growing group of class IId

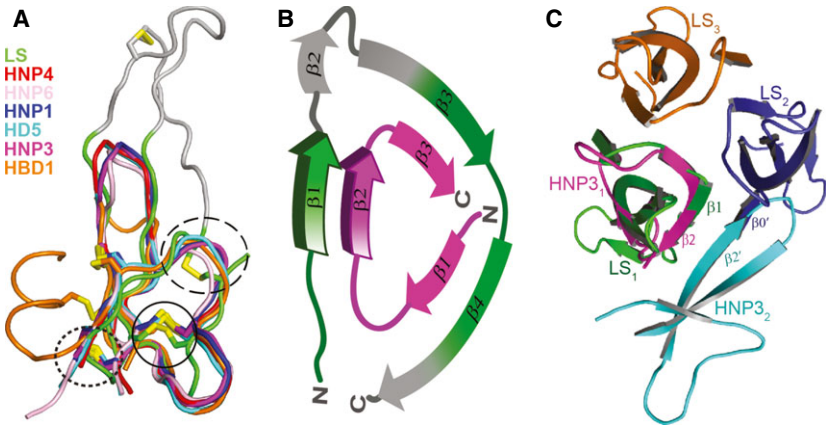

Fig. 8. LS harbors defensin-like structural module. (A) Structural superposition of LS (green) with representative defensins (details are given in Experimental procedures). The structurally conserved disulfide is marked by a solid-line circle, and the additional unmatched region of LS is shown in gray. The dotted-line circle and the dashed-line circle show the conserved covalent connectivity at structurally equivalent positions corresponding to disulfide bonds present in LS and defensins. (B) Graphical representation of structural alignment of α-defensin HNP3 (pink) with LS (green). The β-strands in LS and in HNP3 involved in self-association are highlighted. (C) Structural superposition of the monomeric units of the LS trimer (LS_1) and the HNP3 dimer ($HNP3_1$) shows that the structurally equivalent β-strand is utilized for self-association in both LS and HNP3. Different monomeric units of the two peptides are indicated as subscripts ($LS_{1–3}$ and $HNP3_{1–2}$). All structural superpositions were carried out with COOT [21].

bacteriocins. In addition to possessing a broad spectrum of antimicrobial activity, LS also emerges as a promising AMP against nonmultiplying bacteria, which constitute a major cause of recurrence of chronic infections. Intriguingly, the amino acid composition of LS is unlike that reported for bacteriocins, and it is rich in cysteines, tyrosines, histidines, arginines, aspartates, and glutamates. The higher proportions of polar residues and cysteines in the peptide are closer to the amino acid profile observed in AMPs of higher eukaryotes [19]. Crystal structure analysis indicates that the monomer with an atypical residue composition and termini 'stapled' by disulfides may further self-associate into a tightly packed trimer. The presence of disulfides and an all-β conformation places LS structurally with β-AMPs, which include class IIa bacteriocins, defensins, and cyclotides. A cursory structural analysis of the LS monomer with disulfide connectivity of C^{I}–C^{V}, C^{II}–C^{IV} and C^{III}–C^{VI} suggests its resemblance to β-defensins.

Systematic structural comparison performed with PDBeFold [20], with 50% set as acceptable for query and target in the matching process, and disregarding connectivity, returned several hits corresponding to HDs. Among the linear HDs, including the α-defensins and β-defensins, which are highly structurally homologous, with a core rmsd of < 1 Å, human neutrophil peptide (HNP)4 was one of the top hits, with a *Q*-score of 0.38 and a *Z*-score of 4.5. Although the backbone Cα superimposition of HNP4 with LS by PDBeFold yielded an rmsd of 1.6 Å over 28 aligned residues, manual inspection of the structures indicated the possibility of an alternative superimposition. In fact, using SSM SUPERPOSE in COOT 0.6.2 [21], we observed better structural alignment, revealing striking overall structural similarities between LS and defensins [22,23] (Fig. 8A). In the case of β-defensins, except for the short α-helix at the N terminus [24], the β-sheet core region superimposed well with the LS backbone. The structural superposition of LS with defensins also revealed the importance of disulfide positioning in maintaining the overall tertiary structure of the peptide. The disulfide bond structurally equivalent to C^{II}–C^{IV}, i.e. between Cys5 and Cys34 in LS, is conserved in all close structural homologs (solid-line circle in Fig. 8A). The disulfide Cys3–Cys45 bond in LS, corresponding to C^{I}–C^{V}, is a regular peptide bond in defensins (dashed-line circle in Fig. 8A), and the peptide bond between Asn36 and Gly37 in LS is replaced by a structurally equivalent disulfide bond in defensins (dotted-line circle in Fig. 8A). Thus, defensins can be visualized as circular permutations of truncated LS, as shown by the graphical representation in Fig. 8B.

Dimerization and higher-order oligomerization is an observed phenomenon in defensins [25]. Typically, dimers are observed in the crystal structure of human β-defensins (HBDs); for example, HBD3 forms symmetrical dimers through strand β2 [26], the HBD2 dimer involves a six-stranded β-sheet utilizing strand β1, and a quaternary octameric assembly is observed

in the crystal forms [27], and a topologically distinct aromatic side chain-mediated dimer is observed in the case of HBD1 [24]. However, solution experiments suggest that, unlike HBD3, which forms dimers at low concentrations, HBD1 [26] and HBD2 [28] are monomeric, and HBD2 dimers are observed at 30 mg·mL^{-1}. In the case of α-defensins, dimerization in HNPs is mediated by the association of β2-strands from the subunits to form an antiparallel β-sheet at the interaction interface (indicated by strands β2 and β2′ of $HNP3_1$ and $HNP3_2$ monomers in Fig. 8C) [22]. The observed trimerization of LS in the crystal structure can be compared with the oligomerization in defensins. The LS trimeric state in the crystal structure shows intermolecular hydrogen bonding between strand β1 of one subunit and strand β0′ of another subunit (Fig. 8C). Such an arrangement with inclusion of an intersubunit strand to the four-stranded sheet in the monomer leading to β-sheet expansion at the interface may also be viewed as quasi-domain swapping [29]. Like HBD1 and HBD2, the monomeric defensins, LS exists as a monomer at low concentrations, and is likely to form trimers at higher concentrations. Molecular-level characterization of LS in the current study demonstrates it to be the first structural homolog of an HD-like AMP in bacteria. Thus, LS, with eukaryotic features, exemplifies the adaptive evolution known to occur in components of innate immunity, and in particular it provides a potential link to the evolution of defensins. In addition to enhancing our understanding of diverse structure–activity relationships in bacteriocins, the structural analyses of LS will help in the *de novo* design and/or engineering of potent antimicrobials.

Experimental procedures

LS purification

LS was purified from the supernatant of a liter culture of *Brevibacillus* sp. GI-9 strain grown in nutrient broth (Hi-Media) at 30 °C for 48 h, as described previously [11], with a few minor modifications. In brief, LS secreted in the cell-free broth was allowed to bind to Diaion HP20 resin (Sigma), and eluted with methanol in a batch mode. The methanol-eluted fraction was evaporated and redissolved in MilliQ water, and this active crude extract was passed through a 30-kDa protein concentrator (Millipore). The filtrate thus obtained was the active fraction, and was subjected to a final purification step with size exclusion chromatography (Shodex KW802.5) and/or cation exchange chromatography. The purity, disulfide status and oligomeric nature of the purified peptide were analyzed by subjecting native and 1 mM TCEP-reduced samples to 18% Tris/glycine or 16% Tris/tricine SDS/PAGE, on a Superdex peptide HR 10/300 size exclusion column equipped with an AKTA purifier unit (GE Healthcare), and by mass spectrometry analysis with ABSCIEX, 5800 MALDI TOF-TOF.

Nonmultiplying cell preparation

Antibiotic-sensitive cells of *P. aeruginosa* MTCC 1934 and *S. aureus* MTCC 1430 were obtained from the Microbial Type Culture Collection and Gene Bank, Chandigarh, India. *P. aeruginosa* and *S. aureus* cells were grown in nutrient broth medium (250 mL, inoculated with 10 mL of overnight cultures) at 37 °C with shaking at 150 rpm for 7 days [30]. The 7-day-old cultures were washed twice with PBS, resuspended in PBS, and incubated at 37 °C for 10 days with shaking at 150 rpm. Cell viability was checked by counting colony-forming units (CFUs) each day. The resuspended culture showed a decrease in CFU number in the first 3 days, and remained constant thereafter, at 3×10^6 and 2.8×10^5 CFU·mL^{-1} for *P. aeruginosa* and *S. aureus*, respectively. The cells that had been incubated for 4 days were used as stocks of nonmultiplying cells after confirmation of their dormancy state by overnight treatment of cells (10^6 or 10^7 CFU·mL^{-1}) with 2 X MIC of Amp and by comparison of regrowth curves with that of vegetative cells. Regrowth was performed in a volume of 300 μL in a honeycomb (Bioscreen HC2, Finland) plate, with a starting culture at a $D_{600\ nm}$ of 0.025 and continuous monitoring at $D_{600\ nm}$ on the Bioscreen C MBR (Oy Growth Curves).

Nonmultiplying cell-killing activity assay

To 100 μL of a nonmultiplying cell suspension (10^6 or 10^7 CFU·mL^{-1} in PBS) of *P. aeruginosa* and *S. aureus* in a sterile 1.5-mL centrifuge tubes, different antibiotics, i.e. Amp (Bio Basic), PMB, and NS (Sigma), and purified LS were added at 2 X MIC and 10 X MIC. Cells were incubated at 37 °C overnight, and then washed (three or four times) with PBS to remove excess antibiotics. Washed cells were serially diluted in PBS and plated on nutrient agar plates for counting of CFUs. An untreated sample was processed in the same way in a control experiment.

Hemolytic assay

RBCs were separated from a few milliliters of whole blood of New Zealand white rabbits by centrifugation at 900 ***g*** for 10 min, and washed twice with PBS. All animal protocols were performed according to the National Regulatory Guidelines issued by the Committee for the Purpose of Control and Supervision of Experiments on Animals, Ministry of Environment & Forests (Government of India).

The washed cells were resuspended in PBS to achieve 2×10^8 cells·mL^{-1} [31]. For hemolysis, cells were treated with LS (~ 5–550 μg·mL^{-1}) and incubated in a CO_2 incubator for 24 h at 37 °C. Cell-free supernatant was separated by centrifugation (900 ***g***, 15 min), and absorbance was read at 541 nm. Triton X-100 (0.1% v/v; G-Biosciences) and PBS were used as positive and negative controls, respectively.

TEM

Actively growing cell suspensions of *P. aeruginosa* and *S. aureus* (at a $D_{600\ nm}$ of 0.2) were pelleted and resuspended in same volume of PBS. Aliquots of 100 μL were treated with LS at 1 X MIC (2.0 μg and 0.5 μg for *P. aeruginosa* and *S. aureus*, respectively), and incubated at 37 °C for 1 h. After treatment, cells on a 300-mesh carbon-coated copper grid (Polybioscience) were negatively stained with 0.1% (w/v) sodium phosphotungstate (Sigma) in water for 1 min, as described previously [32], and observed under a JEOL JEM 2100, 200-kV transmission electron microscope.

Fluorescence microscopy

Fresh cells of *P. aeruginosa* and *S. aureus* were prepared in PBS as mentioned earlier, and 100-μL aliquots were treated with LS at 2 X MIC (4.0 μg and 1.0 μg, respectively) for 1 h at 37 °C. Cells were stained with fluorescent dyes according to the procedure described in [32], with a few modifications. After treatment, cells were collected by centrifugation (5000 ***g***, 5 min), resuspended in 100 μL of PBS containing 6.0 μg·mL^{-1} FITC (Sigma) or CTC (Sigma), and incubated for 30 min at room temperature or 37 °C. Cells were washed three or four times with PBS to remove unbound/surface-bound dye. In the case of CTC staining, cells were incubated on poly(L-lysine)-coated coverslips for 45 min at 30 °C, and unbound cells were removed by washing with PBS. The coated cells were incubated with DAPI solution (10 μg·mL^{-1}; Sigma) for 15 min, and washed again with 10 mM sodium phosphate (pH 7.4). DAPI-treated cells were stained with FITC in a triple-staining experiment. However, we often observed that cell damage was caused by the longer procedure of multiple staining. Therefore, the FITC single-labeling experiment was also independently performed as described above. Slides were prepared by fixing cells on microscopic glass slides by air drying, and washing with PBS to remove any traces of the dye. Mowiol-DABCO antifade-mounting medium (Sigma) was used to mount the coverslip over the slide before visualization. An Eclipse 80i (Nikon) fluorescence microscope was used for imaging. Control slides of untreated cells were prepared and observed under the same conditions.

Crystallization

Initial crystallization trials were performed with the 96-well sitting drop vapor diffusion method at 18 °C. Commercial screens from Hampton Research and Molecular Dimensions were used to screen peptide in 50 mM sodium acetate (pH 4.5) at two different concentrations, i.e. 3.5 mg·mL^{-1} and 2.3 mg·mL^{-1}. Cubical crystals were observed after 2 months in several conditions. Native data were collected from crystals grown in 0.1 M Tris (pH 8.5) and 3 M NaCl. Iodine derivatives were made by soaking crystals grown in 0.1 M sodium acetate trihydrate (pH 4.6) and 2 M NaCl for 1 min in mother liquor containing 0.5 M sodium iodide. No cryoprotectant was added, as crystals were grown in high salt concentrations (> 2 M NaCl).

Data collection and structure solution

Native and iodine derivative crystals of LS diffracted to ~ 2.0 Å resolution at home source (λ = 1.5418 Å) at 100 K. Data were collected with an MAR345 image plate detector. Diffraction data were processed with IMOSFLM [33] and scaled with SCALA [34]. As there was no structural homolog of LS in the Protein Data Bank (PDB), iodine derivative crystals were made by use of the quick soak halide method [35]. The structure was solved with the SIRAS protocol of the AUTO-RICKSHAW server [36]. Briefly, the data were prepared and converted for use in AUTO-RICKSHAW by using programs of the CCP4 suite [34]. Data preparation for the SIRAS protocol, substructure determination and initial phase calculations were carried out with the SHELX C/D/E software suite [37]. All of the nine heavy atoms requested were found with SHELXD [37]. Ninety-six per cent of the model was built with ARP/WARP [38]. Several rounds of manual model building with COOT [21] and refinement cycles with PHENIX [39] were performed until R/R_{free} of 0.212/0.272 was achieved. This iodine derivative structure (excluding iodine atoms and water molecules) was used as a model to refine the native structure by using rigid body refinement at the initial stage of the refinement cycle in PHENIX. The native structure was refined to final R/R_{free} of 0.196/0.227 after several rounds of manual model building with COOT and refinement cycles with PHENIX. The structure has excellent geometry, as 97.87% and 2.13% of residues were in the preferred and allowed regions, respectively, of the Ramachandran plot. Figures were created with PYMOL [40]. The electrostatic surface representation was analyzed with UCSF CHIMERA [41]. A single PDB file for the crystallographic trimer was generated by merging coordinates of the three-fold symmetry-related chains to carry out the secondary structure assignments for the trimeric assembly. The structural superposition of LS (4OZK) with representative defensins, i.e. HNP1 (3GNY), HNP3 (1DFN), HNP4 (1ZMM), HNP6 (1ZMQ), HD5 (1ZMP), and β-defensin [HBD1 (1IJV)], were carried out with COOT.

CD and fluorescence measurement

Far UV–CD spectra (195–250 nm) of 10 μM native and 1 mM TCEP-reduced LS in MilliQ water were recorded at 25 °C on a Jasco J815 spectropolarimeter equipped with a temperature control unit, in a 0.2-cm pathlength cuvette. To analyze protein stability, a thermal denaturation experiment was performed. A native LS sample was heated at a rate of 1 °C·min^{-1} from 25 °C to 90 °C, and the far UV–CD spectrum was measured at every 10 °C interval.

The fluorescence spectrum of 2 μM purified LS (native and 1 mM TCEP-reduced samples in MilliQ water) was measured on a PTI QM-40 spectrofluorimeter at 25 °C with the excitation set at 295 nm.

Acknowledgements

P. K. Singh thanks Dr Subash Pawar for TEM imaging, Uday Agarwal for MALDI measurements, and Piyush Baindara for help with hemolysis assays. We thank the X-ray, 3D, mass spectrometry, electron microscopy and protein instrumentation facilities at CSIR-IMTECH. This work was supported by financial assistance from CSIR and DBT, Government of India, to S. Korpole, and CSIR funding to K. G. Thakur and B. Krishnan. P. K. Singh and V. Solanki are supported by a CSIR research fellowship. B. Krishnan is a recipient of the DBT-Ramalingaswami fellowship.

Author contributions

K. G. Thakur, B. Krishnan and S. Korpole designed and supervised research. P. K. Singh and S. Sharma purified LS and performed activity measurements. P. K. Singh performed microscopy and in-solution characterization, and contributed to writing of the paper. V. Solanki crystallized the peptide. K. G. Thakur determined the crystal structure, and performed comparative structural analysis. P. K. Singh, K. G. Thakur, B. Krishnan and S. Korpole analyzed data. K. G. Thakur, B. Krishnan and S. Korpole wrote the paper.

References

1 Keren I, Kaldalu N, Spoering A, Wang Y & Lewis K (2004) Persister cells and tolerance to antimicrobials. *FEMS Microbiol Lett* **230**, 13–18.
2 Coates AR & Hu Y (2008) Targeting non-multiplying organisms as a way to develop novel antimicrobials. *Trends Pharmacol Sci* **29**, 143–150.
3 Peschel A & Sahl HG (2006) The co-evolution of host cationic antimicrobial peptides and microbial resistance. *Nat Rev Microbiol* **4**, 529–536.
4 Zasloff M (2002) Antimicrobial peptides of multicellular organisms. *Nature* **415**, 389–395.
5 Fjell CD, Hiss JA, Hancock RE & Schneider G (2012) Designing antimicrobial peptides: form follows function. *Nat Rev Drug Discovery* **11**, 37–51.
6 Fox JL (2013) Antimicrobial peptides stage a comeback. *Nat Biotechnol* **31**, 379–382.
7 Yeaman MR & Yount NY (2003) Mechanisms of antimicrobial peptide action and resistance. *Pharmacol Rev* **55**, 27–55.
8 Brogden KA (2005) Antimicrobial peptides: pore formers or metabolic inhibitors in bacteria? *Nat Rev Microbiol* **3**, 238–250.
9 Arnett E & Seveau S (2011) The multifaceted activities of mammalian defensins. *Curr Pharm Des* **17**, 4254–4269.
10 Cotter PD, Ross RP & Hill C (2013) Bacteriocins – a viable alternative to antibiotics? *Nat Rev Microbiol* **11**, 95–105.
11 Singh PK, Chittpurna, Ashish, Sharma V, Patil PB & Korpole S (2012) Identification, purification and characterization of laterosporulin, a novel bacteriocin produced by *Brevibacillus* sp. strain GI-9. *PLoS One* **7**, e31498.
12 Mangoni ML, Papo N, Barra D, Simmaco M, Bozzi A, Di Giulio A & Rinaldi AC (2004) Effects of the antimicrobial peptide temporin L on cell morphology, membrane permeability and viability of *Escherichia coli*. *Biochem J* **380**, 859–865.
13 Tina KG, Bhadra R & Srinivasan N (2007) PIC: Protein Interactions Calculator. *Nucleic Acids Res* **35**, W473–W476.
14 Hider RC, Kupryszewski G, Rekowski P & Lammek B (1988) Origin of the positive 225-230 nm circular dichroism band in proteins. Its application to conformational analysis. *Biophys Chem* **31**, 45–51.
15 Takekiyo T, Wu L, Yoshimura Y, Shimizu A & Keiderling TA (2009) Relationship between hydrophobic interactions and secondary structure stability for Trpzip beta-hairpin peptides. *Biochemistry* **48**, 1543–1552.
16 Manning MC & Woody RW (1987) Theoretical determination of the CD of proteins containing closely packed antiparallel beta-sheets. *Biopolymers* **26**, 1731–1752.
17 Sreerama N & Woody RW (2003) Structural composition of betaI- and betaII-proteins. *Protein Sci* **12**, 384–388.
18 Fancy DA, Denison C, Kim K, Xie Y, Holdeman T, Amini F & Kodadek T (2000) Scope, limitations and mechanistic aspects of the photo-induced cross-linking of proteins by water-soluble metal complexes. *Chem Biol* **7**, 697–708.
19 Mishra B & Wang G (2012) The importance of amino acid composition in natural AMPs: an evolutional,

structural, and functional perspective. *Front Immunol* **3**, 221.
20 Krissinel E & Henrick K (2004) Secondary-structure matching (SSM), a new tool for fast protein structure alignment in three dimensions. *Acta Crystallogr D Biol Crystallogr* **60**, 2256–2268.
21 Emsley P & Cowtan K (2004) Coot: model-building tools for molecular graphics. *Acta Crystallogr D Biol Crystallogr* **60**, 2126–2132.
22 Hill CP, Yee J, Selsted ME & Eisenberg D (1991) Crystal structure of defensin HNP-3, an amphiphilic dimer: mechanisms of membrane permeabilization. *Science* **251**, 1481–1485.
23 Szyk A, Wu Z, Tucker K, Yang D, Lu W & Lubkowski J (2006) Crystal structures of human alpha-defensins HNP4, HD5, and HD6. *Protein Sci* **15**, 2749–2760.
24 Hoover DM, Chertov O & Lubkowski J (2001) The structure of human beta-defensin-1: new insights into structural properties of beta-defensins. *J Biol Chem* **276**, 39021–39026.
25 Dhople V, Krukemeyer A & Ramamoorthy A (2006) The human beta-defensin-3, an antibacterial peptide with multiple biological functions. *Biochim Biophys Acta* **1758**, 1499–1512.
26 Schibli DJ, Hunter HN, Aseyev V, Starner TD, Wiencek JM, McCray PB Jr, Tack BF & Vogel HJ (2002) The solution structures of the human beta-defensins lead to a better understanding of the potent bactericidal activity of HBD3 against *Staphylococcus aureus*. *J Biol Chem* **277**, 8279–8289.
27 Hoover DM, Rajashankar KR, Blumenthal R, Puri A, Oppenheim JJ, Chertov O & Lubkowski J (2000) The structure of human beta-defensin-2 shows evidence of higher order oligomerization. *J Biol Chem* **275**, 32911–32918.
28 Sawai MV, Jia HP, Liu L, Aseyev V, Wiencek JM, McCray PB Jr, Ganz T, Kearney WR & Tack BF (2001) The NMR structure of human beta-defensin-2 reveals a novel alpha-helical segment. *Biochemistry* **40**, 3810–3816.
29 Liu Y & Eisenberg D (2002) 3D domain swapping: as domains continue to swap. *Protein Sci* **11**, 1285–1299.
30 Hu Y, Shamaei-Tousi A, Liu Y & Coates A (2010) A new approach for the discovery of antibiotics by targeting non-multiplying bacteria: a novel topical antibiotic for staphylococcal infections. *PLoS One* **5**, e11818.
31 Ghosh JK, Shaool D, Guillaud P, Ciceron L, Mazier D, Kustanovich I, Shai Y & Mor A (1997) Selective cytotoxicity of dermaseptin S3 toward intraerythrocytic *Plasmodium falciparum* and the underlying molecular basis. *J Biol Chem* **272**, 31609–31616.
32 Marcellini L, Giammatteo M, Aimola P & Mangoni ML (2010) Fluorescence and electron microscopy methods for exploring antimicrobial peptides mode(s) of action. *Methods Mol Biol* **618**, 249–266.
33 Leslie AGW, & Powell HR (2007) Processing Diffraction Data with Mosflm in Evolving Methods for Macromolecular Crystallography pp. 41–51, Springer, the Netherlands.
34 CCP4 (1994) The CCP4 suite: programs for protein crystallography. *Acta Crystallogr D Biol Crystallogr* **50**, 760–763.
35 Dauter Z, Dauter M & Rajashankar KR (2000) Novel approach to phasing proteins: derivatization by short cryo-soaking with halides. *Acta Crystallogr D Biol Crystallogr* **56**, 232–237.
36 Panjikar S, Parthasarathy V, Lamzin VS, Weiss MS & Tucker PA (2005) Auto-rickshaw: an automated crystal structure determination platform as an efficient tool for the validation of an X-ray diffraction experiment. *Acta Crystallogr D Biol Crystallogr* **61**, 449–457.
37 Sheldrick GM (2008) A short history of SHELX. *Acta Crystallogr A* **64**, 112–122.
38 Cohen SX, Morris RJ, Fernandez FJ, Ben Jelloul M, Kakaris M, Parthasarathy V, Lamzin VS, Kleywegt GJ & Perrakis A (2004) Towards complete validated models in the next generation of ARP/wARP. *Acta Crystallogr D Biol Crystallogr* **60**, 2222–2229.
39 Echols N, Grosse-Kunstleve RW, Afonine PV, Bunkoczi G, Chen VB, Headd JJ, McCoy AJ, Moriarty NW, Read RJ, Richardson DC *et al.* (2012) Graphical tools for macromolecular crystallography in PHENIX. *J Appl Crystallogr* **45**, 581–586.
40 DeLano WL (2002) The PyMOL Molecular Graphics System. DeLano Scientifics, San Carlos, CA, USA.
41 Pettersen EF, Goddard TD, Huang CC, Couch GS, Greenblatt DM, Meng EC & Ferrin TE (2004) UCSF Chimera–a visualization system for exploratory research and analysis. *J Comput Chem* **25**, 1605–1612.